CMIP6 Intermodel Spread in Interhemispheric Asymmetry of Tropical Climate Response to Greenhouse Warming: Extratropical Ocean Effects

YU-FAN GENG,[a] SHANG-PING XIE,[b] XIAO-TONG ZHENG,[a] SHANG-MIN LONG,[c] SARAH M. KANG,[d] XIAOPEI LIN,[e] AND ZI-HAN SONG[a]

[a] *Physical Oceanography Laboratory, Institute for Advanced Ocean Studies, Ocean University of China and Qingdao National Laboratory for Marine Science and Technology, Qingdao, China*
[b] *Scripps Institution of Oceanography, University of California San Diego, La Jolla, California*
[c] *College of Oceanography, Key Laboratory of Marine Hazards Forecasting, Ministry of Natural Resources, Key Laboratory of Ministry of Education for Coastal Disaster and Protection, Hohai University, Nanjing, China*
[d] *School of Urban and Environmental Engineering, Ulsan National Institute of Science and Technology, Ulsan, Republic of Korea*
[e] *Frontier Science Center for Deep Ocean Multispheres and Earth System and Physical Oceanography Laboratory, Ocean University of China, and Qingdao National Laboratory for Marine Science and Technology, Qingdao, China*

(Manuscript received 14 July 2021, in final form 22 March 2022)

ABSTRACT: Tropical climate response to greenhouse warming is to first order symmetric about the equator but climate models disagree on the degree of latitudinal asymmetry of the tropical change. Intermodel spread in equatorial asymmetry of tropical climate response is investigated by using 37 models from phase 6 of the Coupled Model Intercomparison Project (CMIP6). In the simple simulation with CO_2 increase at 1% per year but without aerosol forcing, this study finds that intermodel spread in tropical asymmetry is tied to that in the extratropical surface heat flux change related to the Atlantic meridional overturning circulation (AMOC) and Southern Ocean sea ice concentration (SIC). AMOC or Southern Ocean SIC change alters net energy flux at the top of the atmosphere and sea surface in one hemisphere and may induce interhemispheric atmospheric energy transport. The negative feedback of the shallow meridional overturning circulation in the tropics and the positive low cloud feedback in the subtropics are also identified. Our results suggest that reducing the intermodel spread in extratropical change can improve the reliability of tropical climate projections.

KEYWORDS: Asymmetry; Climate change; Energy budget/balance; Model comparison

1. Introduction

Deep convection in the intertropical convergence zone (ITCZ) drives the atmospheric circulation and helps shape regional climate around the world. Anthropogenic radiative forcing is expected to change spatiotemporal distributions of tropical rainfall, but climate models disagree on tropical rainfall change (Ma and Xie 2013; Xie et al. 2015; Long et al. 2016). It is important to identify sources of and reduce the uncertainty in projecting tropical rainfall change.

Diagnostically, tropical rainfall change can be decomposed into the responses of water vapor and atmospheric circulation (Seager et al. 2010; Huang et al. 2013). Under global warming, rainfall change due to the increase in water vapor follows the present climatological rainfall distribution (Chou and Neelin 2004; Held and Soden 2006; Chou et al. 2009), known as the wet-get-wetter mechanism. Uneven sea surface temperature (SST) warming in space (Xie 2020) results in the change in spatial distribution of atmospheric circulation. The SST warming pattern effect is known as the warmer-get-wetter mechanism, with rainfall increase where the SST warming exceeds the tropical mean, and vice versa (Xie et al. 2010). In the multimodel ensemble (MME) mean, the annual tropical rainfall mainly increases in the northern Indian Ocean and the equatorial Pacific and Atlantic, following a warmer-get-wetter pattern (Chadwick et al. 2013).

Beyond the ensemble mean, several studies have investigated the intermodel spread in tropical rainfall change under global warming. Moisture budget analyses reveal that the major intermodel discrepancy in tropical rainfall projections is rooted in the intermodel spread in the dynamic contribution due to atmospheric circulation change (Ma and Xie 2013; Kent et al. 2015; Long et al. 2016; Weller et al. 2019). The uncertainty in the SST warming pattern is further identified as the major cause of the intermodel spread in tropical rainfall projections over oceans (Chadwick 2016). Long et al. (2016) identify a tight coupling between the intermodel variations in SST warming pattern and tropical circulation change from intermodel singular value decomposition (SVD) analysis. In the zonal mean, the first mode is a meridional dipole in SST with an interhemispheric anomalous Hadley cell. Long et al. (2016) suggested that the tropical asymmetric mode is associated with the shortwave radiative flux change at the top of the atmosphere (TOA) in the subtropics and midlatitudes. The present study explores the possibility that intermodel spread in tropical climate change may originate from extratropical sea surface heat flux.

Extratropical energy perturbations can influence tropical rainfall and atmospheric circulation (Kang 2020; Kang et al. 2020; Hwang et al. 2021). Zonal-mean energetics theory relates

Supplemental information related to this paper is available at the Journals Online website: https://doi.org/10.1175/JCLI-D-21-0541.s1.

Corresponding author: Shang-Ping Xie, sxie@ucsd.edu

DOI: 10.1175/JCLI-D-21-0541.1

© 2022 American Meteorological Society. For information regarding reuse of this content and general copyright information, consult the AMS Copyright Policy (www.ametsoc.org/PUBSReuseLicenses).

Brought to you by UNIVERSITY OF CALIFORNIA San Diego - SIO LIBRARY 0219 SERIALS | Unauthenticated | Downloaded 07/02/22 12:17 AM UTC

the cross-equatorial atmospheric energy transport to the interhemispheric contrast in atmospheric net energy input from the TOA and surface. Ocean circulation is important for cross-equatorial energy transport (Kay et al. 2016; Hawcroft et al. 2017; Xiang et al. 2018). In response to a hemispheric perturbation (e.g., anthropogenic aerosols in the Northern Hemisphere), the Atlantic meridional overturning circulation (AMOC) responds to damp the cross-equatorial asymmetry of tropical climate change (Tomas et al. 2016; Kang et al. 2019, 2021), while AMOC change itself can act as a driver of meridional asymmetry as in water-hosing experiments in the context of the Dansgaard-Oeschger cycle and Heinrich events (Zhang and Delworth 2005; Timmermann et al. 2007). In addition, the wind-driven ocean circulation change damps the extratropical influence on the ITCZ shift (Schneider 2017; Green and Marshall 2017; Kang et al. 2018). Long et al. (2016) explored the TOA and sea surface flux patterns associated with the CMIP5 intermodel spread in the ITCZ asymmetry but the results are inconclusive because of large uncertainties in aerosol radiative forcing of the RCP4.5 scenario.

The present study investigates the sources of intermodel spread in tropical climate change, focusing on the interhemispheric asymmetry in the state-of-the-art CMIP6 multimodel ensemble. To sidestep the uncertainty in radiative forcing due to anthropogenic aerosols, we analyze the transient greenhouse warming experiment. Climate responses to greenhouse gas forcing are only weakly asymmetric about the equator. For a tropical-mean warming of 3°C, the CMIP6 MME-mean asymmetry in SST change is only 0.17°C while the intermodel standard deviation (0.20°C) is equally large (Fig. 1c).

In transient greenhouse warming, the subpolar ocean is far from a thermal equilibrium, with the largest ocean heat uptake in the Southern Ocean and North Atlantic (Shi et al. 2018) due to the mean upwelling and AMOC slowdown (Marshall et al. 2015), respectively. Ocean heat uptake in either region can cause large meridional asymmetry in SST warming (Hwang et al. 2017; Liu et al. 2020; Hu et al. 2022). Our hypothesis is that diversity in representing these and other possible sources among CMIP6 models leads to intermodel spread in the ITCZ asymmetry. From our analysis, the AMOC change indeed emerges as a likely source of intermodel spread in the interhemispheric asymmetry of tropical climate change. In the Southern Ocean, however, sea ice concentration (SIC) poleward of the mean ocean upwelling turns out to be the most correlated source of intermodel spread in the ITCZ asymmetry. In the tropics, our analysis implies a negative feedback due to the shallow ocean meridional overturning circulation (MOC) and a positive feedback due to low cloud radiative effect at the TOA.

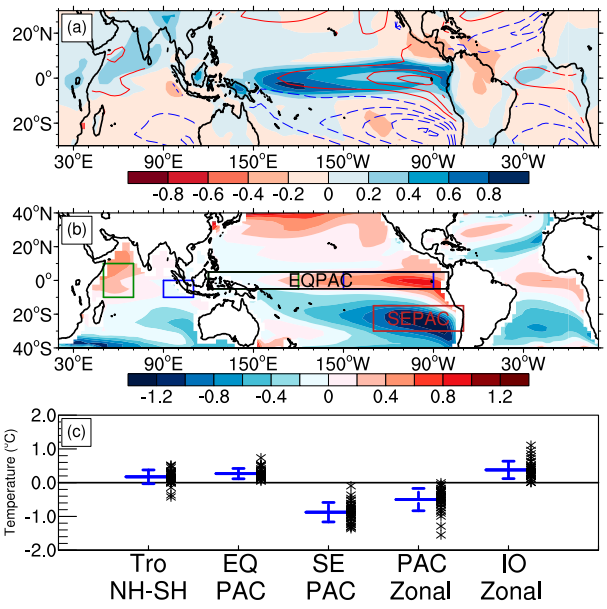

FIG. 1. (a) The ensemble-mean tropical rainfall change (shading; mm day^{-1}). The red solid contours are positive deviation of the annual-mean ΔSST from the tropical mean of 3.0°C, and the blue dashed contours are negative (with 0.3°C interval; between ±0.2°C omitted). (b) The ensemble-mean relative SST warming pattern (the deviation of the annual-mean ΔSST from the tropical mean; shading). (c) Five ΔSST indices among 37 CMIP6 models. The blue bar is the ensemble mean with one standard deviation. Each black asterisk denotes the value of each individual model. Each column shows the index in different regions. The leftmost index is tropical NH (0°–20°N) minus SH (20°S–0°) ΔSST. The second index is the equatorial Pacific ΔSST [EQPAC; the black box in (b): 5°S–5°N, 120°E–80°–80°W] minus the tropical mean (20°S–20°N). The middle index is the southeast Pacific ΔSST [SEPAC; the red box in (b): 15°–30°S, 70°–130°W] minus the tropical mean. The fourth index is the Pacific Ocean zonal ΔSST (PAC Zonal), calculated by the equatorial western Pacific ΔSST (the green box in the Pacific Ocean: 5°S–5°N, 120°E–180°) minus the equatorial eastern Pacific ΔSST (the blue box in the Pacific Ocean: 5°S–5°N, 90°–150°W). The rightmost index is the Indian Ocean zonal ΔSST (IO Zonal), calculated by the equatorial western Indian ΔSST (the green box in the Indian Ocean: 10°S–10°N, 50°–70°E) minus the equatorial eastern Indian ΔSST (the blue box in the Indian Ocean: 0°–10°S, 90°–110°E).

2. Data and methods

a. CMIP6

The monthly mean outputs from 37 CMIP6 models in preindustrial control (piControl) and 1%CO2 simulations are used to study intermodel spread in tropical climate projections. The 1%CO2 scenario begins from a piControl state with atmospheric CO_2 concentration increasing at 1% per year. Note that some variables are unavailable in some models (Table 1). Climate change is calculated by subtracting the last 100-yr mean in the piControl run from the 50-yr (years 101–150) mean in the 1%CO2 run. All atmospheric outputs are interpolated onto a common grid of 2.5° × 2.5° and oceanic outputs onto 1° × 1°. Only the first-member run of each model is analyzed. All changes are normalized by the tropical mean SST warming in each model.

CMIP intermodel spread is a mixture of internal variability and model physics diversity. Some models improve in complexity from the previous generation while others have changed

Brought to you by UNIVERSITY OF CALIFORNIA San Diego - SIO LIBRARY 0219 SERIALS | Unauthenticated | Downloaded 07/02/22 12:17 AM UTC

TABLE 1. Names and institutions of 37 CMIP6 models used in this study. Note that percentage cloud cover (cl), near-surface humidity (huss), near-surface wind speed (sfcWind), sea ice area percentage (siconc), eastward near-surface wind (uas), northward near-surface wind (vas), and seawater Y velocity (vo) outputs are unavailable in some models.

	Model name	Institution (country)	Unavailable outputs
1	ACCESS-CM2	CSIRO-ARCCSS (Australia)	cl
2	ACCESS-ESM1-5	CSIRO (Australia)	cl
3	AWI-CM-1-1-MR	AWI (Germany)	cl, siconc, vo
4	BCC-CSM2-MR	BCC (China)	siconc
5	BCC-ESM1	BCC (China)	huss, siconc
6	CAMS-CSM1-0	CAMS (China)	huss
7	CESM2-WACCM	NCAR (United States)	uas, vas
8	CESM2	NCAR (United States)	uas, vas
9	CIESM	THU (China)	uas, vas, sfcWind, siconc
10	CMCC-CM2-SR5	CMCC (Italy)	
11	CMCC-ESM2	CMCC (Italy)	
12	CNRM-CM6-1-HR	CNRM-CERFACS (France)	cl, siconc, vo
13	CNRM-CM6-1	CNRM-CERFACS (France)	siconc
14	CNRM-ESM2-1	CNRM-CERFACS (France)	cl
15	CanESM5	CCCma (Canada)	cl
16	E3SM-1-0	E3SM-Project LLNL (United States)	uas, vas
17	EC-Earth3-Veg	EC-Earth Consortium	cl
18	EC-Earth3	EC-Earth Consortium	cl
19	FGOALS-f3-L	CAS (China)	siconc
20	FGOALS-g3	CAS (China)	uas, vas, sfcWind
21	GFDL-CM4	NOAA-GFDL (United States)	
22	GFDL-ESM4	NOAA-GFDL (United States)	cl, vo
23	GISS-E2-1-G	NASA-GISS (United States)	siconc
24	GISS-E2-1-H	NASA-GISS (United States)	vo
25	GISS-E2-2-G	NASA-GISS (United States)	siconc
26	INM-CM4-8	INM (Russia)	cl, vo
27	INM-CM5-0	INM (Russia)	cl
28	IPSL-CM6A-LR	IPSL (France)	
29	MIROC-ES2L	MIROC (Japan)	
30	MIROC6	MIROC (Japan)	
31	MPI-ESM-1-2-HAM	MPI-M (Germany)	
32	MPI-ESM1-2-HR	MPI-M (Germany)	
33	MPI-ESM1-2-LR	MPI-M (Germany)	
34	MRI-ESM2-0	MRI (Japan)	
35	NESM3	NUIST (China)	huss, sfcWind
36	NorCPM1	NCC (Norway)	cl, sfcWind, vo
37	SAM0-UNICON	SNU (South Korea)	uas, vas

much across generations. Although shared shortcomings in model physics cannot be assessed, identifying sources of intermodel spread is useful for improving models and the projections. In this study, the effect of internal variability is not evaluated separately but likely substantially suppressed by averaging across 37 models.

b. Water vapor budget

Rainfall change in response to global warming can be diagnostically decomposed into thermodynamic and dynamic components (Emori and Brown 2005; Seager et al. 2010; Bony et al. 2013). Based on the water vapor budget equation in Seager et al. (2010), rainfall change can be approximated as follows (Huang et al. 2013; Long et al. 2016; Geng et al. 2020):

$$\Delta P = \frac{1}{\rho_w g}(\omega\Delta q + \Delta\omega q), \tag{1}$$

where P and ρ_w are rainfall and the density of water, respectively; ω and q denote the pressure velocity at 500 hPa and surface specific humidity in the present climatology, respectively, and Δ denotes change under global warming. Here we multiply the 500-hPa pressure velocity by -1 to make ω positive upward.

We further linearize the thermodynamic (ΔP_t) and dynamic (ΔP_d) components separately as follows:

$$\Delta P_t = \frac{1}{\rho_w g}(\omega + \omega')(\Delta q + \Delta q') \approx \frac{1}{\rho_w g}(\omega\Delta q + \omega'\Delta q + \omega\Delta q'), \tag{2}$$

$$\Delta P_d = \frac{1}{\rho_w g}(\Delta\omega + \Delta\omega')(q + q') \approx \frac{1}{\rho_w g}(\Delta\omega q + \Delta\omega' q + \Delta\omega q'), \tag{3}$$

where ωq represents the MME mean climatology, Δ indicates climate change, and the prime denotes the deviation

Brought to you by UNIVERSITY OF CALIFORNIA San Diego - SIO LIBRARY 0219 SERIALS | Unauthenticated | Downloaded 07/02/22 12:17 AM UTC

in individual models from the ensemble mean. In our analyses, the prime denotes the effect of intermodel spread in each term.

c. *Intermodel SVD analysis*

We perform an intermodel SVD analysis with the space–model field instead of the common space–time field. Intermodel SVD analysis is used to identify the coupled spatial patterns of two variables in previous studies (Wang et al. 2014; Long and Xie 2015; Long et al. 2016; Chen et al. 2019). The comprehensive description of the intermodel SVD method can be found in Abe et al. (2011) and Shiogama et al. (2011). In this study, the intermodel SVD analysis is performed between the zonal-mean changes in the tropical SST and atmospheric circulation, following Long et al. (2016) for CMIP5 RCP4.5.

3. Ensemble-mean changes

First, we analyze the MME-mean changes in SST and rainfall (Fig. 1). Relative SST warming (the deviation of the tropical mean warming of 3.0°C) pattern is shown in Fig. 1b. Annual-mean SST change displays enhanced equatorial warming in the Pacific and Atlantic Oceans, with an Indian Ocean dipole (IOD)-like warming pattern in the tropical Indian Ocean (Fig. 1b). The tropical SST change also shows a warming minimum in the southeast Pacific (SEPAC). Under global warming, annual-mean tropical rainfall mainly increases in the equatorial Pacific and Atlantic, and the northwest Indian Ocean (Fig. 1a), following the warmer-get-wetter pattern (Xie et al. 2010). Tropical rainfall decreases as SST warming weakens south of the equator, especially in the SEPAC.

Following Christensen et al. (2013), we develop indices to track patterns of SST change (Fig. 1c). From the right, the first ΔSST index is the zonal difference in the equatorial Indian Ocean, tracking the IOD-like pattern with reduced warming in the east (Fig. 1b). The second index denotes the zonal difference in the equatorial Pacific (EQPAC), indicating an El Niño–like SST warming pattern in most models. The reduced warming in the SEPAC and enhanced warming in the EQPAC are robust across models. The leftmost ΔSST index concerns the tropical Northern Hemisphere (NH) minus Southern Hemisphere (SH) difference. Ensemble-mean SST warming is only weakly asymmetric, consistent with greenhouse gas forcing. On a tropical-mean SST increase of 3°C, the cross-equatorial asymmetry is 0.17°C in the ensemble mean but the intermodel standard deviation is as large. In fact, several models even show larger warming in the SH than NH. Next, we move to investigate the sources of intermodel spread in the tropical interhemispheric asymmetry.

4. Intermodel spread in tropical rainfall change

Intermodel spread in rainfall change is defined as the intermodel standard deviation of $\Delta P'$ (the prime denotes deviations from the ensemble mean). Tropical rainfall change features a large intermodel spread in the climatological rainy regions (Fig. 2a), including the South Pacific convergence zone (SPCZ) and the ITCZ. The robust intermodel spread in rainfall change normalized by local climatological rainfall is confined in the middle and eastern equatorial Pacific over tropical oceans (not shown). Then we decompose the intermodel spread in the thermodynamic (ΔP_t) and dynamic (ΔP_d) components into two parts separately. For the thermodynamic component, the intermodel spread in ω ($\omega'\Delta q$; Fig. 2b) is much larger than that in Δq ($\omega\Delta q'$; not shown). For the dynamic component, on the other hand, the intermodel spread in $\Delta\omega$ ($\Delta\omega' q$; Fig. 2c) is much larger than that in q ($\Delta\omega q'$; not shown). The contribution of $\Delta\omega'$ is much larger in magnitude than that of ω' to the spread in rainfall projections, indicating that the intermodel spread in atmospheric circulation change ($\Delta\omega$) dominates that in tropical rainfall change. Due to the opposite effects of increased moisture and weakened mean circulation on rainfall change (Chadwick et al. 2013), the intermodel spread in atmospheric circulation change (Fig. 2c) is larger than that in rainfall change (Fig. 2a). Consistent with the results in CMIP3 (Ma and Xie 2013) and CMIP5 (Kent et al. 2015; Long et al. 2016) intermodel spread analyses, the atmospheric circulation change continues to show large differences among CMIP6 models.

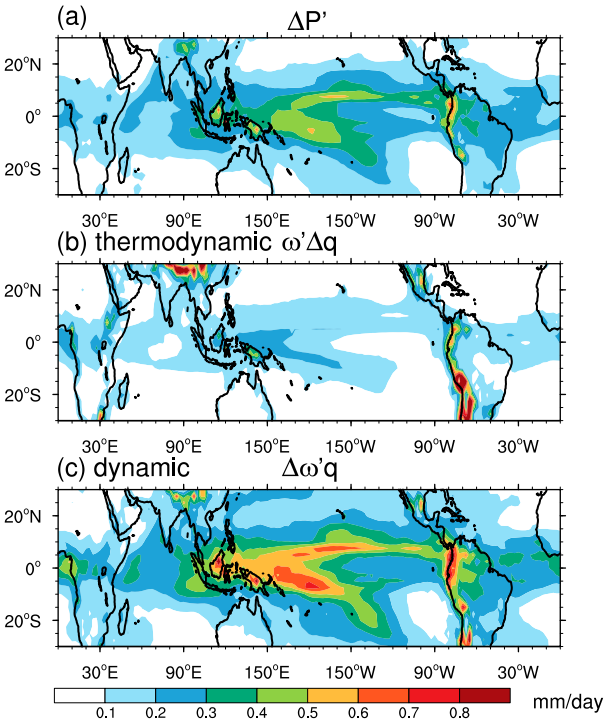

FIG. 2. Intermodel standard deviations in (a) rainfall change $\Delta P'$, (b) thermodynamic component $\omega'\Delta q$, and (c) dynamic component $\Delta\omega' q$. The prime denotes deviations from the ensemble mean. The ensemble mean is calculated as the absolute value.

As the major source of intermodel spread in tropical rainfall change, the atmospheric circulation change is mainly governed by the SST warming pattern over tropical oceans. We conduct the intermodel SVD analysis between the SST and atmospheric circulation changes in the CMIP6 1%CO2 run.

Brought to you by UNIVERSITY OF CALIFORNIA San Diego - SIO LIBRARY 0219 SERIALS | Unauthenticated | Downloaded 07/02/22 12:17 AM UTC

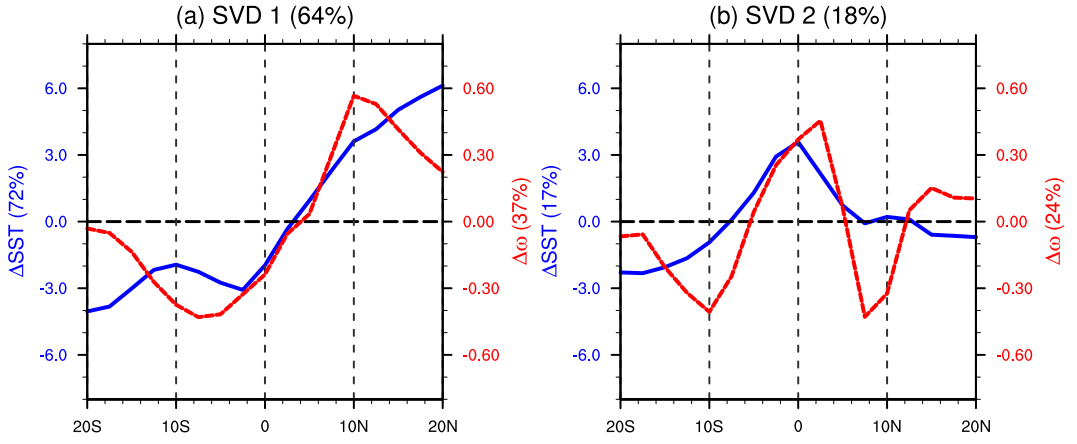

FIG. 3. (a),(b) The first two modes of intermodel SVD analysis between tropical zonal-mean $\Delta\omega'$ (10^2 Pa day^{-1}) and $\Delta SST'$ (10^{-2} °C). The blue solid lines denote $\Delta SST'$, and the red dashed lines denote $\Delta\omega'$. The prime denotes deviations from the ensemble mean.

In the zonal mean, the first two SVD modes show an interhemispheric dipole asymmetry and an equatorial peak, respectively (Fig. 3), consistent with the CMIP5 results. The regression of the zonal-mean rainfall change against PC1 also displays the meridional dipole (not shown). The first mode explains 37% and 72% of the intermodel variances in $\Delta\omega'$and $\Delta SST'$, respectively. The PC1s of $\Delta\omega'$ and $\Delta SST'$ display a high correlation relationship ($r = 0.79$; see Fig. S1 in the online supplemental material), illustrating a tight coupling between the intermodel variations in SST warming and tropical circulation change. In the following discussion, the interhemispheric asymmetry mode refers to larger SST warming in the northern tropics than the southern tropics as shown in Fig. 3a.

Tropical SST pattern indices (Fig. 1c) are found to be useful in describing the intermodel spread of tropical rainfall change (Grose et al. 2014). The tropical NH–SH ΔSST index is highly correlated with the SVD PC1 ($r = 0.97$; Table 2). The SVD PC2 (Fig. 3b) is correlated with the EQPAC ΔSST index at $r = 0.61$.

5. Sources and feedbacks of intermodel spread in tropical asymmetry

Figure 4 shows the zonal-mean atmospheric streamfunction change regressed against the SVD PC1. A larger warming in NH than SH is accompanied by an anomalous cross-equatorial Hadley circulation with the rising branch displaced into the NH. We define the 500-hPa zonal-mean streamfunction change on the equator to track the cross-equatorial anomalous Hadley cell. The Hadley index is highly correlated with the tropical interhemispheric difference in ΔSST ($r = -0.87$), illustrating a tight coupling between the intermodel variations in SST warming pattern and Hadley cell change.

Anomalous southward atmospheric energy transport across the equator needs to balance the energy flux gain of the atmospheric column at the TOA and surface in the NH (Kang et al. 2008). Figure 5a shows the PC1 regressed zonally integrated TOA ($\Delta Q'_{TOA}$) downward and surface ($\Delta Q'_{sfc}$) upward net heat flux changes into the atmospheric column (the prime denotes the MME spread). The terms $\Delta Q'_{TOA}$ and $\Delta Q'_{sfc}$ offset each other in the tropics, while the flux change poleward of 45° (Fig. 5b) seems to cause a cross-equatorial energy

TABLE 2. The correlations (Corr) between the tropical NH–SH ΔSST index (Tro NH-SH) and PC1 and other ΔSST indices.

Corr	PC1	EQPAC	SEPAC	PAC zonal	IO zonal
Tro NH-SH	0.97	−0.07	−0.79	0.40	0.47

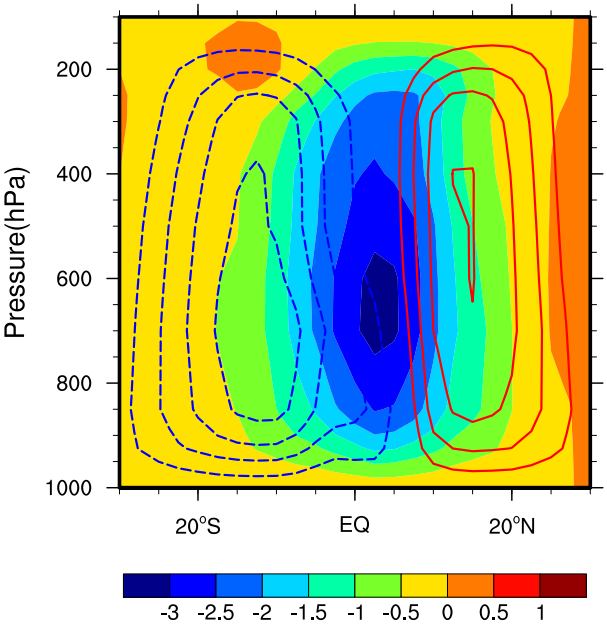

FIG. 4. The regression of zonal-mean streamfunction change against PC1 (shading; 10^9 kg s^{-1}). The climatological streamfunction is in contours (contour interval is 2×10^{10} kg s^{-1}).

Brought to you by UNIVERSITY OF CALIFORNIA San Diego - SIO LIBRARY 0219 SERIALS | Unauthenticated | Downloaded 07/02/22 12:17 AM UTC

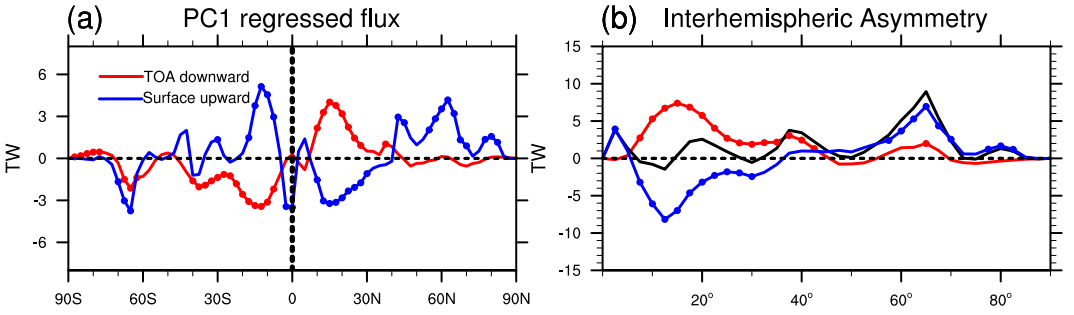

FIG. 5. (a) Regressions of zonally integrated TOA downward (ΔQ_{TOA}; red line) and surface upward (ΔQ_{sfc}; blue line) net heat flux changes against the PC1, with the interhemispheric asymmetry (NH minus SH) in (b). The black line in (b) is the sum of ΔQ_{TOA} and ΔQ_{sfc}. Dotted marks indicate where the regression passes a t test at the 95% significance level.

transport consistent with the anomalous atmospheric Hadley circulation (Fig. 4). The interhemispheric asymmetry is calculated as NH minus SH. In Fig. 5b, $\Delta Q'_{\mathrm{sfc}}$ features a large interhemispheric asymmetry in the mid- to high latitudes, with contributions from both the NH and SH (Fig. 5a). In the extratropics $\Delta Q'_{\mathrm{sfc}}$ is most positively correlated with the interhemispheric asymmetry mode and has the opposite effect in the tropics. The sum of $\Delta Q'_{\mathrm{TOA}}$ and $\Delta Q'_{\mathrm{sfc}}$ shows a maximum in the mid- to high latitudes, indicating that the major source of the intermodel spread in the tropical interhemispheric asymmetry lies most likely in the extratropics, especially in the mid- to high latitudes.

The $\Delta Q'_{\mathrm{TOA}}$ and $\Delta Q'_{\mathrm{sfc}}$ regression result (Fig. 5b) is different from that in Fig. 8a of Long et al. (2016). Based on the CMIP5 RCP4.5 run, Long et al. (2016) suggested that the intermodel spread in TOA shortwave radiation in the subtropics and midlatitudes—suggestive of the uncertainty in aerosol radiative effect—drives that in tropical asymmetry. They found that $\Delta Q'_{\mathrm{sfc}}$ is not significant in the mid- to high latitudes (their Fig. 8a), so Long et al. (2016) cannot conclusively show the extratropical $\Delta Q'_{\mathrm{sfc}}$ effects. Regarding our regression result, $\Delta Q'_{\mathrm{TOA}}$ is nearly zero north of 40°N (Fig. 5a), likely because we have excluded the aerosol effect that could complicate the TOA radiation in the NH. This allows identifying the extratropical ocean heat uptake as likely origins of intermodel spread in the tropical asymmetry.

a. Extratropical origins

We examine the origin of surface heat flux change related to the cross-equatorial Hadley cell. Figure 6a shows that $\Delta Q'_{\mathrm{sfc}}$ is large in the mid- to high-latitude North Atlantic. The $\Delta Q'_{\mathrm{sfc}}$ increases over the Gulf Stream and the Irminger and Norwegian Seas, with a conspicuous maximum in the Labrador Sea, which plays a vital role in AMOC variability (Menary et al. 2016, 2020). Given that net surface heat flux change (ΔQ_{sfc}) is balanced by the ocean heat transport divergence and storage under global warming (Xie et al. 2010), we consider the AMOC change as the dominant source of the interhemispheric asymmetry in the extratropical NH.

The AMOC has a significant influence on global climate through its meridional heat transport. All models predict a weakened AMOC in a warmer climate, resulting in global and regional impacts (Liu et al. 2020), although the degree of AMOC weakening varies considerably among the models (Cheng et al. 2013; Weijer et al. 2020). Figure 7 shows the MME mean of meridional overturning streamfunction change zonally integrated in the Atlantic Ocean. The ensemble mean shows an AMOC weakening under global warming, consistent with previous studies. The regressed meridional overturning streamfunction change is positive with a deep structure in the North Atlantic (Fig. 7), indicating that the positive phase of the interhemispheric asymmetry mode with a northward displaced ITCZ corresponds to models of a weak AMOC decline under global warming.

Besides the distinct increase in the North Atlantic, $\Delta Q'_{\mathrm{sfc}}$ increases over the Arctic Ocean between 30° and 120°E, yet partially offset with the negative anomaly in the Greenland Sea (Fig. 6b). In the extratropics of SH, $\Delta Q'_{\mathrm{sfc}}$ decreases over the Southern Ocean between 60° and 70°S (Fig. 6), related to the Southern Ocean SIC change. The Southern Ocean takes up a large amount of anthropogenic heat (Shi et al. 2018) due to the upwelling of deep water that delays local SST warming (Marshall et al. 2015). The ocean heat uptake due to the mean upwelling mainly occurs north of 60°S in the Southern Ocean (see Fig. S2 in the online supplemental material; Shi et al. 2018), but the MME spread is displaced considerably south of 60°S (Fig. 5a) due to the large intermodel difference in SIC change. The Southern Ocean sea ice rapidly decreases in model simulations in tandem with the SST warming (Zhang et al. 2019), as supported by the ensemble-mean result (Fig. 8). Antarctic sea ice loss has an important impact on tropical climate responses (England et al. 2020). The regressed SIC change against the tropical PC1 is positive between 60° and 70°S, indicating that models with a small Southern Ocean SIC decline under global warming is likely to project a northward shift of the ITCZ. Due to a slow loss of Southern Ocean sea ice, the ocean releases less heat flux change to the atmosphere south of 60°S (Fig. 6b). Meanwhile, local downward $\Delta Q'_{\mathrm{TOA}}$ decreases (Fig. 5a) because sea ice reflects shortwave solar radiation back into space. Energy perturbations at both the TOA and surface cause the ITCZ to shift northward.

We define an ΔAMOC index following Cheng et al. (2013) and Shi et al. (2018) and an ΔSIC index. Table 3 shows the correlations between the ΔAMOC and ΔSIC and with local

Brought to you by UNIVERSITY OF CALIFORNIA San Diego - SIO LIBRARY 0219 SERIALS | Unauthenticated | Downloaded 07/02/22 12:17 AM UTC

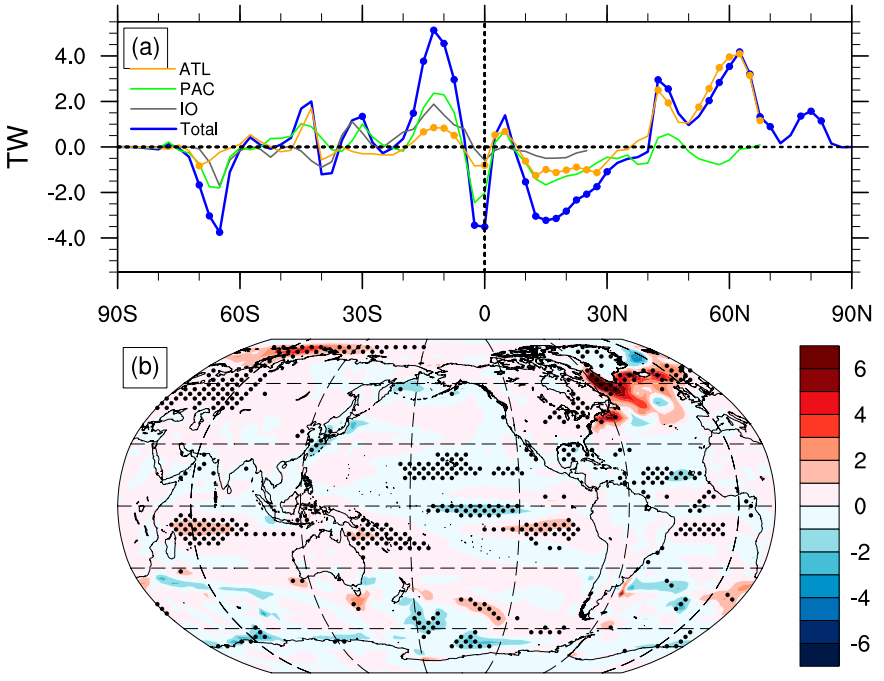

FIG. 6. (a) Regressions of ΔQ_{sfc} zonally integrated in the Atlantic Ocean (ATL; orange line), Pacific Ocean (PAC; green line), and Indian Ocean (IO; gray line) and the total ΔQ_{sfc} (blue line) against the PC1. Dotted marks in orange and blue lines indicate where the regression passes a t test at the 95% significance level. (b) Spatial pattern of the regression of the ΔQ_{sfc} (W m^{-2}) against the PC1. Stippling indicates where the regression passes a t test at the 90% significance level.

$\Delta Q'_{sfc}$ in each region. The AMOC–SIC correlation is not very high, suggesting that they are not coupled. Each change shows a high negative correlation with local $\Delta Q'_{sfc}$. Besides, both indices are highly correlated with the SVD PC1. They can also reproduce the regressed $\Delta Q'_{sfc}$ and $\Delta Q'_{TOA}$ results (Fig. S3), similar to the PC1 regressed results (Fig. 5). Therefore, the AMOC and Southern Ocean SIC changes are identified as the extratropical features most correlated with the tropical interhemispheric asymmetry in MME spread.

Additionally, the SIC change is closely related to the climatological SIC in the piControl run (Fig. 9a), suggesting that the sea ice change could be influenced by the simulated sea ice climatology (Kajtar et al. 2021). The MME spread in AMOC change does not show a robust correlation with the AMOC in the piControl run (Fig. 9b). Previous studies found that AMOC decline under global warming is stronger in the models with a stronger mean state (Gregory et al. 2005;

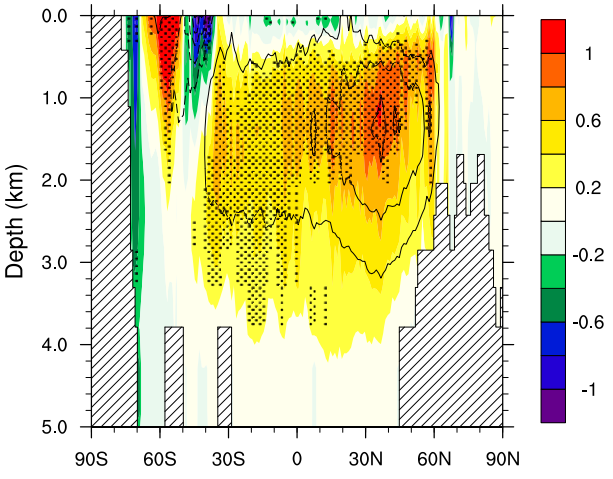

FIG. 7. Regression of the meridional overturning streamfunction change zonally integrated in the Atlantic Ocean against the PC1 (shading; Sv). Solid contours denote negative values of the MME mean of meridional overturning streamfunction change zonally integrated in the Atlantic Ocean and dashed contours denote positive values (with 1-Sv intervals). Stippling indicates where the regression passes a t test at the 95% significance level.

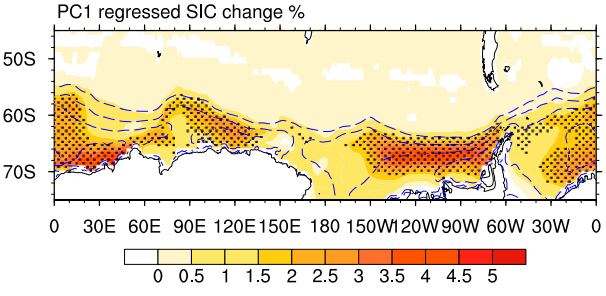

FIG. 8. Regression of SIC change against the PC1 (shading). Stippling indicates where the regression passes a t test at the 95% significance level. Dashed blue contours denote MME mean of Southern Ocean SIC change (with 2% interval).

Brought to you by UNIVERSITY OF CALIFORNIA San Diego - SIO LIBRARY 0219 SERIALS | Unauthenticated | Downloaded 07/02/22 12:17 AM UTC

TABLE 3. The correlations between ΔAMOC index and ΔSIC index, and with each local surface ΔQ_{sfc} deviation from the ensemble mean (ΔQ_{AMOC} 57.5°–70°N; ΔQ_{SO} 65°–70°S). The ΔAMOC index is the deviation of the maximum meridional overturning streamfunctions at 30°N in the warming climate and the piControl. The ΔSIC index is the 60°–70°S mean SIC change normalized by the tropical mean SST warming in each model.

Indices	Correlations
ΔAMOC index and ΔSIC index	0.37, $p = 0.07$
ΔQ_{AMOC} and ΔQ_{SO}	−0.39, $p = 0.06$
ΔAMOC index and PC1	0.67
ΔSIC index and PC1	0.68
ΔAMOC index and ΔQ_{AMOC}	0.77
ΔSIC index and ΔQ_{SO}	−0.91

Weaver et al. 2012), while the relationship cannot be reproduced by all CMIP6 models (Weijer et al. 2020).

b. Tropical and subtropical feedbacks

Beyond the effects of ΔQ_{sfc} in the mid- to high latitudes on the tropics, we find a high negative correlation in the interhemispheric asymmetries of upward ΔQ_{sfc} and the downward net TOA heat flux change (ΔQ_{TOA}) meridionally integrated in the tropics and subtropics (5°–30°) among 37 CMIP6 models ($r = -0.79$; not shown). We consider that this remarkable intermodel consistency indicates the large cancellation between the surface negative feedback effects (e.g., the shallow oceanic MOC damping effect) and the TOA positive feedback effects (e.g., the positive low cloud and water vapor feedbacks).

In the tropics, the trade wind change associated with the anomalous cross-equatorial Hadley cell implies a positive wind–evaporation–SST (WES) feedback (Fig. 10). The WES feedback is instrumental in mediating the tropical asymmetric adjustments to the extratropical forcing. Note that $\Delta Q'_{sfc}$ increases in the tropics of SH and decreases in the NH, indicating a damping effect of the ocean circulation change on the interhemispheric asymmetry mode (Fig. 5a).

In the tropics, $\Delta Q'_{sfc}$ is due to the shallow MOC change. The shallow MOC is driven by the trade winds and is coupled to the anomalous cross-equatorial Hadley circulation. In the interhemispheric asymmetry mode, northward shift of the ITCZ is accompanied by a cross-equatorial northward surface wind (Fig. 10), inducing a weakening of the easterly wind stress in the NH and a strengthening in the SH. The easterly wind stress change causes southward Ekman flow in both hemispheres. Therefore, an anomalous cross-equatorial oceanic cell transports energy and damps ITCZ shifts (Green and Marshall 2017; Kang et al. 2018; Green et al. 2019). Figure 11a shows the MME mean of meridional overturning streamfunction change zonally integrated from the Indo-Pacific Ocean. The ensemble mean result indicates that the shallow MOC decreases in a warmer climate, with a stronger weakening north of the equator. Figure 11b shows the PC1 regressed shallow MOC change representing the MME spread. The shallow MOC south of the equator strengthens and north of the equator weakens. Figure 11c shows meridionally integrated $\Delta Q'_{sfc}$ from the North Pole. The surface net flux is balanced by ocean heat divergence (OHD) and storage. Given that the spatial pattern of ΔQ_{sfc} is mainly shaped by ΔOHD (Hu et al. 2020), meridionally integrated ΔQ_{sfc} is approximately the northward ocean heat transport. The regressed shallow MOC change indicates a southward cross-equatorial ocean heat transport (Fig. 11c) and damps the northward shift of the ITCZ. Thus, the shallow

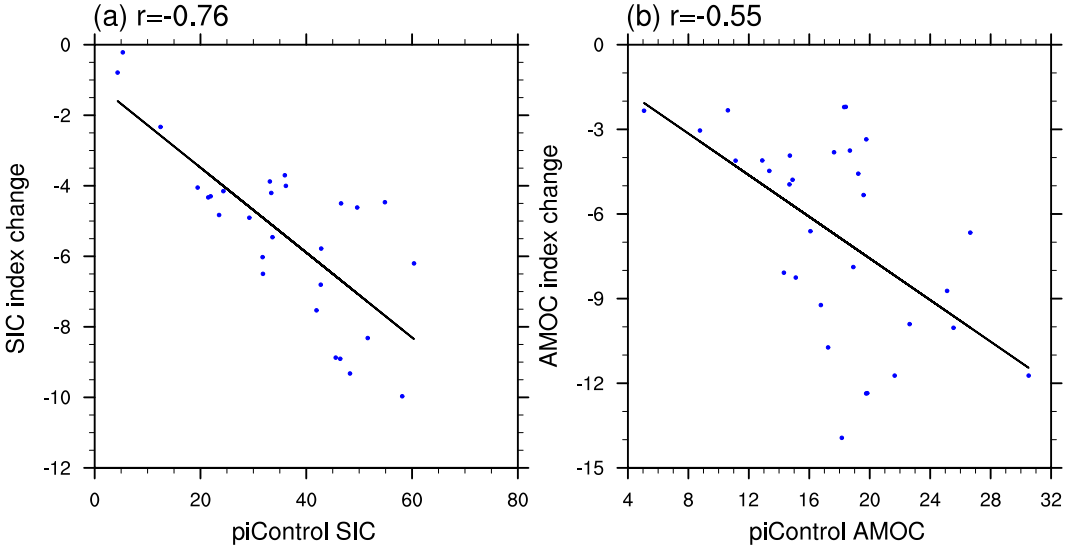

FIG. 9. Scatterplots of (a) SIC index change vs climatological mean in piControl run and (b) AMOC index change vs climatological mean in piControl run. The AMOC index change is defined as the change of the maximum meridional overturning streamfunction at 30°N, and the SIC index change is calculated as the change of the 60°–70°S mean SIC.

Brought to you by UNIVERSITY OF CALIFORNIA San Diego - SIO LIBRARY 0219 SERIALS | Unauthenticated | Downloaded 07/02/22 12:17 AM UTC

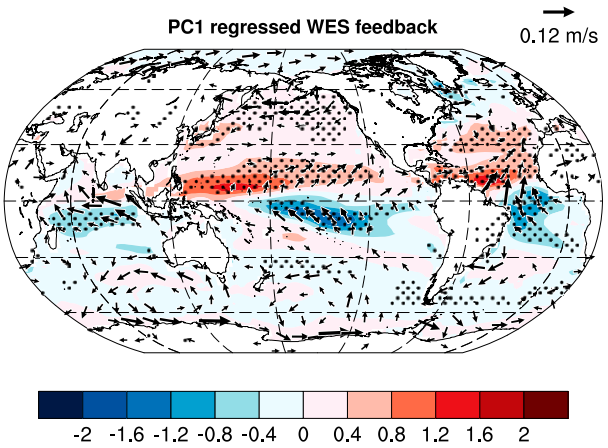

FIG. 10. Regression of the WES feedback effect (estimated as the latent heat change due to wind speed change; shading) and surface wind change (vectors; values < 0.04 m s^{-1} are omitted) against the PC1. Stippling indicates where the regression passes a t test at the 95% significance level.

MOC effect acts as a negative feedback to the interhemispheric asymmetry.

The term $\Delta Q'_{\mathrm{TOA}}$, on the other hand, represents a positive feedback on the tropical interhemispheric asymmetry mode (Fig. 5b). We further decompose $\Delta Q'_{\mathrm{TOA}}$ into clear-sky and cloud components. The clear-sky component has a positive contribution in the tropics (not shown), possibly due to the water vapor feedback (Soden and Held 2006; Clark et al. 2018). Figure 12 shows spatial patterns of TOA cloud components. The regressed cloud component of TOA shortwave flux change increases in the northeast Atlantic, North Pacific, equatorial central Pacific, and Southern Ocean between 60° and 70°S, and mainly decreases in the equatorial eastern Pacific, southwest Pacific, and the subtropical eastern oceans of SH, especially in the SEPAC (Fig. 12a). Besides, the regressed cloud component of TOA longwave flux change partly cancels out that of TOA shortwave flux change in the tropics (Fig. 12b), leading to a prominent interhemispheric asymmetry of TOA total cloud component in the extratropics (Fig. 12c). Therefore, the cloud feedback in $\Delta Q'_{\mathrm{TOA}}$ is positive and amplifies the interhemispheric asymmetry mode. Low clouds mostly reflect the shortwave radiation, so in the eastern oceans of the subtropical SH the spatial pattern of the regressed low cloud fraction change (Fig. 12d) matches that of the cloud component of TOA shortwave flux change (Fig. 12a). Because of the positive low-cloud radiative feedback, the tropical NH–SH ΔSST index is highly correlated with the SEPAC ΔSST index ($r = -0.79$; Table 2).

The low cloud reduction in the North Atlantic (Fig. 12d) may be associated with a decrease in static stability resulting from a positive AMOC anomaly. The low cloud fraction

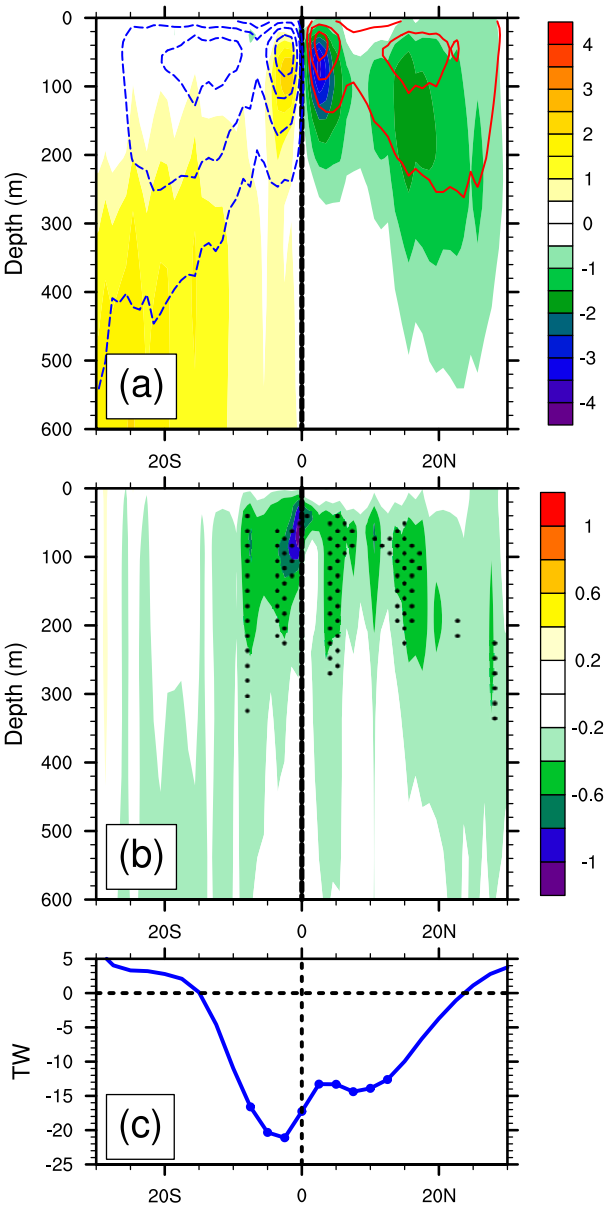

FIG. 11. (a) Multimodel ensemble mean of meridional overturning streamfunction change (Sv) zonally integrated from the Indian Ocean to the Pacific Ocean (shading), along with the climatological meridional overturning streamfunction (contours; interval of 10 Sv). Positive values (red and solid contours) indicate a clockwise circulation and negative values (blue and dashed contours) indicate a counterclockwise circulation. (b) Regression of the meridional overturning streamfunction change zonally integrated from the Indian Ocean to the Pacific Ocean against the PC1. Stippling indicates where the regression passes a t test at the 95% significance level. (c) Meridionally integrated upward surface net flux change (regressed zonally integrated ΔQ_{sfc}) from 90°N. Dotted marks indicate where the regression passes a t test at the 95% significance level.

Brought to you by UNIVERSITY OF CALIFORNIA San Diego - SIO LIBRARY 0219 SERIALS | Unauthenticated | Downloaded 07/02/22 12:17 AM UTC

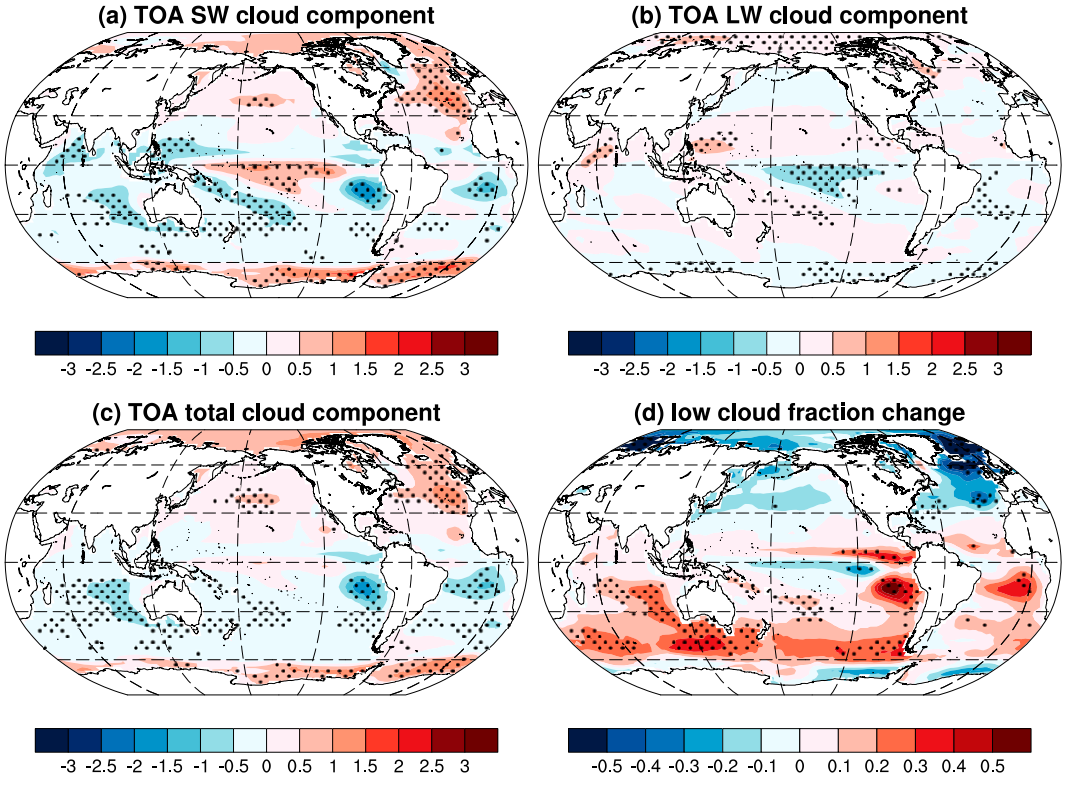

FIG. 12. Spatial patterns of the regressions of cloud components of (a) TOA ΔSW, (b) ΔLW, (c) total cloud component (W m^{-2}), and (d) low cloud fraction change (>700 hPa) against the PC1. Stippling indicates where the regression passes a *t* test at the 95% significance level.

change over the Southern Ocean has a negligible effect on the TOA cloud component possibly because the cloud top is mainly in the midlevels of the atmosphere (Fig. S4). The cloud component of TOA shortwave flux change (Fig. 12a) south of 60°S is opposite to the TOA net flux change (Fig. 5a) due to the blocking effect of cloud on surface shortwave reflection.

6. Summary and discussion

We have investigated the major sources of intermodel spread in tropical climate change under greenhouse warming based on 37 CMIP6 models. The atmospheric circulation change is identified as the major source of intermodel spread in tropical rainfall change, consistent with previous studies (Ma and Xie 2013; Kent et al. 2015; Long et al. 2016). The MME-mean SST warming is nearly symmetric about the equator; with a tropical mean warming of 3°C, the NH–SH tropical difference is only 0.17°C. The cross-equatorial asymmetry varies considerably among models. In fact, an interhemispheric asymmetric mode emerges from the SVD analysis of the MME spread between the zonal-mean SST and atmospheric circulation changes. Sources and mechanisms of intermodel spread in tropical interhemispheric asymmetry are further explored.

The MME spread in interhemispheric asymmetry is associated with an anomalous cross-equatorial Hadley cell. The anomalous atmospheric energy transport by the Hadley cell can be understood as resulting from interhemispheric difference in net TOA-surface energy flux into the atmosphere. Therefore, the differences in atmospheric energy flux changes among models account for the intermodel spread in interhemispheric asymmetry of tropical changes. Significantly, the $\Delta Q'_{\mathrm{TOA}}$ and $\Delta Q'_{\mathrm{sfc}}$ anomalies offset each other largely in the tropics, and $\Delta Q'_{\mathrm{sfc}}$ shows a large interhemispheric asymmetry in the mid- to high latitudes.

The extratropical ocean effects on intermodel spread in cross-equatorial asymmetry of tropical climate response are shown schematically in Fig. 13. Our results are obtained by regression against the PC1 of intermodel SVD analysis between the tropical SST and atmospheric circulation changes. Our hypothesis is that the major source of the intermodel spread in the tropical interhemispheric asymmetry is in the extratropics, especially in the mid- to high latitudes. The AMOC and Southern Ocean SIC changes are identified as the extratropical features most correlated with the cross-equatorial asymmetry mode of intermodel variability. We interpret tropical anomalies in TOA and sea surface energy fluxes as feedbacks. The shallow MOC change in the tropics damps the tropical asymmetry, while the low-cloud shortwave radiative feedback in the eastern subtropical oceans in the SH, especially in the SEPAC, amplifies the asymmetry.

A previous analysis of CMIP5 RCP4.5 scenario found that intermodel spread in tropical asymmetry is related to

Brought to you by UNIVERSITY OF CALIFORNIA San Diego - SIO LIBRARY 0219 SERIALS | Unauthenticated | Downloaded 07/02/22 12:17 AM UTC

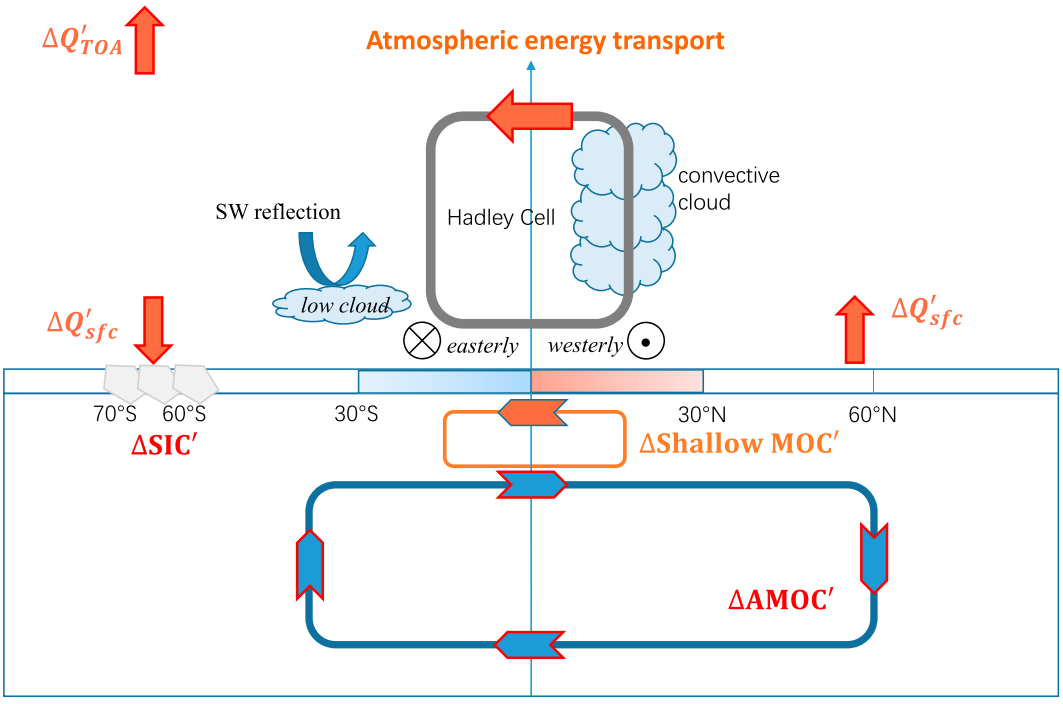

FIG. 13. Schematic of the extratropical ocean effects on intermodel spread in interhemispheric asymmetry. The prime denotes the MME spread. The AMOC and Southern Ocean SIC changes are identified as the dominant extratropical features most correlated with the tropical interhemispheric asymmetry in multimodel ensemble spread in the NH and SH, respectively. Both of them can affect the local surface net energy flux change and may further remotely affect the tropical asymmetry via anomalous atmospheric energy transport. Meanwhile, Southern Ocean SIC change can also affect the local TOA net energy flux change because sea ice reflects shortwave solar radiation back into the TOA. In the tropics, the WES feedback help maintain the asymmetric pattern due to the trade wind change, while the shallow MOC acts as a negative feedback to the interhemispheric asymmetry and damps the ITCZ shift. The effects of convective clouds on shortwave and longwave radiative fluxes are nearly equal. However, low clouds mostly block shortwave radiative flux. The low cloud change in the subtropical SH shows a positive feedback to the tropical asymmetry.

the spread in TOA shortwave radiation in the subtropics and midlatitudes (Fig. 8 of Long et al. 2016). The result resembles that of the CMIP6 historical simulation (Fig. S5), in contrast to our results that instead identify sea surface heat flux in the Southern Ocean and subpolar North Atlantic as the most likely sources. The difference is due to our choice to focus on the 1%CO2 run and sidestep the large uncertainties in aerosol forcing of the RCP4.5 scenario and historical run. Regarding the spread in extratropical surface flux, intermodel variability in Southern Ocean sea ice loss is strongly related to the model SIC climatology, which shows large spread among models. This supports the notion that reducing model bias in climatology improves regional climate projections (Zhou and Xie 2015; Geng et al. 2020). Model resolution affects the paths of North Atlantic currents and hence the simulated AMOC (Hewitt et al. 2020), while low clouds over subtropical oceans have long been flagged as a major uncertainty in radiative feedback (Soden and Held 2006). The statistical relationship between MME spread and the climatology may be used to develop observational constraints on model projections, as has been applied for tropical SST warming patterns (Li et al. 2016a,b; Ying et al. 2019).

Model biases affect future climate projections. For example, the double ITCZ bias may be reduced by improving convective parameterization (Song and Zhang 2018) and may be related to extratropical biases (Hwang and Frierson 2013; Li and Xie 2014). The uncertainty due to internal variability (Hawkins and Sutton 2009; Dai et al. 2015) is not separately investigated here but can be better quantified using large ensemble simulations (Deser et al. 2012, 2020; Kay et al. 2015). The intermodel spread in different emission scenarios and under multiple forcings (including aerosols and ozone) should also be investigated in future studies.

Acknowledgments. We acknowledge the World Climate Research Programme Working Group on Coupled Modeling for coordinating and promoting CMIP6, and the Earth System Grid Federation (ESGF) for archiving the data and providing access. CMIP6 model data can be accessed through the ESGF website (https://esgf-node.llnl.gov/search/cmip6/). Y.F.G. is supported by the National Key Research and Development

Brought to you by UNIVERSITY OF CALIFORNIA San Diego - SIO LIBRARY 0219 SERIALS | Unauthenticated | Downloaded 07/02/22 12:17 AM UTC

Program of China (2018YFA0605702) and S.P.X. by the National Science Foundation (AGS-1934392).

REFERENCES

Abe, M., H. Shiogama, T. Nozawa, and S. Emori, 2011: Estimation of future surface temperature changes constrained using the future–present correlated modes in inter-model variability of CMIP3 multimodel simulations. *J. Geophys. Res.*, **116**, D18104, https://doi.org/10.1029/2010JD015111.

Bony, S., G. Bellon, D. Klocke, S. Sherwood, S. Fermepin, and S. Denvil, 2013: Robust direct effect of carbon dioxide on tropical circulation and regional precipitation. *Nat. Geosci.*, **6**, 447–451, https://doi.org/10.1038/ngeo1799.

Chadwick, R., 2016: Which aspects of CO_2 forcing and SST warming cause most uncertainty in projections of tropical rainfall change over land and ocean? *J. Climate*, **29**, 2493–2509, https://doi.org/10.1175/JCLI-D-15-0777.1.

——, I. Boutle, and G. Martin, 2013: Spatial patterns of precipitation change in CMIP5: Why the rich do not get richer in the tropics. *J. Climate*, **26**, 3803–3822, https://doi.org/10.1175/JCLI-D-12-00543.1.

Chen, C., W. Liu, and G. Wang, 2019: Understanding the uncertainty in the 21st century dynamic sea level projections: The role of the AMOC. *Geophys. Res. Lett.*, **46**, 210–217, https://doi.org/10.1029/2018GL080676.

Cheng, W., J. C. H. Chiang, and D. Zhang, 2013: Atlantic meridional overturning circulation (AMOC) in CMIP5 models: RCP and historical simulations. *J. Climate*, **26**, 7187–7197, https://doi.org/10.1175/JCLI-D-12-00496.1.

Chou, C., and J. D. Neelin, 2004: Mechanisms of global warming impacts on regional tropical precipitation. *J. Climate*, **17**, 2688–2701, https://doi.org/10.1175/1520-0442(2004)017<2688:MOGWIO>2.0.CO;2.

——, ——, C. A. Chen, and J. Y. Tu, 2009: Evaluating the "rich-get-richer" mechanism in tropical precipitation change under global warming. *J. Climate*, **22**, 1982–2005, https://doi.org/10.1175/2008JCLI2471.1.

Christensen, J. H., and Coauthors, 2013: Climate phenomena and their relevance for future regional climate change. *Climate Change 2013: The Physical Science Basis*, T. F. Stocker et al., Eds., Cambridge University Press, 1217–1308, https://doi.org/10.1017/CBO9781107415324.028.

Clark, S. K., Y. Ming, I. M. Held, and P. Phillipps, 2018: The role of the water vapor feedback in the ITCZ response to hemispherically asymmetric forcings. *J. Climate*, **31**, 3659–3678, https://doi.org/10.1175/JCLI-D-17-0723.1.

Dai, A., J. C. Fyfe, S.-P. Xie, and X. Dai, 2015: Decadal modulation of global surface temperature by internal climate variability. *Nat. Climate Change*, **5**, 555–559, https://doi.org/10.1038/nclimate2605.

Deser, C., A. Phillips, V. Bourdette, and H. Y. Teng, 2012: Uncertainty in climate change projections: The role of internal variability. *Climate Dyn.*, **38**, 527–546, https://doi.org/10.1007/s00382-010-0977-x.

——, and Coauthors, 2020: Insights from Earth system model initial-condition large ensembles and future prospects. *Nat. Climate Change*, **10**, 277–286, https://doi.org/10.1038/s41558-020-0731-2.

Emori, S., and S. J. Brown, 2005: Dynamic and thermodynamic changes in mean and extreme precipitation under changed climate. *Geophys. Res. Lett.*, **32**, L17706, https://doi.org/10.1029/2005GL023272.

England, M. R., L. M. Polvani, L. Sun, and C. Deser, 2020: Tropical climate responses to projected Arctic and Antarctic sea-ice loss. *Nat. Geosci.*, **13**, 275–281, https://doi.org/10.1038/s41561-020-0546-9.

Geng, Y.-F., S.-P. Xie, X.-T. Zheng, and C.-Y. Wang, 2020: Seasonal dependency of tropical precipitation change under global warming. *J. Climate*, **33**, 7897–7908, https://doi.org/10.1175/JCLI-D-20-0032.1.

Green, B., and J. Marshall, 2017: Coupling of trade winds with ocean circulation damps ITCZ shifts. *J. Climate*, **30**, 4395–4411, https://doi.org/10.1175/JCLI-D-16-0818.1.

——, ——, and J.-M. Campin, 2019: The 'sticky' ITCZ: Ocean moderated ITCZ shifts. *Climate Dyn.*, **53**, 1–19, https://doi.org/10.1007/s00382-019-04623-5.

Gregory, J. M., and Coauthors, 2005: A model intercomparison of changes in the Atlantic thermohaline circulation in response to increasing atmospheric CO_2 concentration. *Geophys. Res. Lett.*, **32**, L12703, https://doi.org/10.1029/2005GL023209.

Grose, M. R., J. Bhend, S. Narsey, A. Sen Gupta, and J. R. Brown, 2014: Can we constrain CMIP5 rainfall projections in the tropical Pacific based on surface warming patterns? *J. Climate*, **27**, 9123–9138, https://doi.org/10.1175/JCLI-D-14-00190.1.

Hawcroft, M., J. M. Haywood, M. Collins, A. Jones, A. C. Jones, and G. Stephens, 2017: Southern Ocean albedo, inter-hemispheric energy transports and the double ITCZ: Global impacts of biases in a coupled model. *Climate Dyn.*, **48**, 2279–2295, https://doi.org/10.1007/s00382-016-3205-5.

Hawkins, E., and R. Sutton, 2009: The potential to narrow uncertainty in regional climate predictions. *Bull. Amer. Meteor. Soc.*, **90**, 1095–1108, https://doi.org/10.1175/2009BAMS2607.1.

Held, I. M., and B. J. Soden, 2006: Robust responses of the hydrological cycle to global warming. *J. Climate*, **19**, 5686–5699, https://doi.org/10.1175/JCLI3990.1.

Hewitt, H. T., and Coauthors, 2020: Resolving and parameterising the ocean mesoscale in Earth system models. *Curr. Climate Change Rep.*, **6**, 137–152, https://doi.org/10.1007/s40641-020-00164-w.

Hu, S., S.-P. Xie, and W. Liu, 2020: Global pattern formation of net ocean surface heat flux response to greenhouse warming. *J. Climate*, **33**, 7503–7522, https://doi.org/10.1175/JCLI-D-19-0642.1.

——, ——, and S. M. Kang, 2022: Global warming pattern formation: The role of ocean heat uptake. *J. Climate*, **35**, 1885–1899, https://doi.org/10.1175/JCLI-D-21-0317.1.

Huang, P., S.-P. Xie, K. M. Hu, G. Huang, and R. H. Huang, 2013: Patterns of the seasonal response of tropical rainfall to global warming. *Nat. Geosci.*, **6**, 357–361, https://doi.org/10.1038/ngeo1792.

Hwang, Y.-T., and D. M. W. Frierson, 2013: Link between the double-intertropical convergence zone problem and cloud biases over the Southern Ocean. *Proc. Natl. Acad. Sci. USA*, **110**, 4935–4940, https://doi.org/10.1073/pnas.1213302110.

——, S.-P. Xie, C. Deser, and S. M. Kang, 2017: Connecting tropical climate change with Southern Ocean heat uptake. *Geophys. Res. Lett.*, **44**, 9449–9457, https://doi.org/10.1002/2017GL074972.

——, H.-Y. Tseng, K.-C. Li, S. M. Kang, Y.-J. Chen, and J. C. H. Chiang, 2021: Relative roles of energy and momentum fluxes in the tropical response to extratropical thermal forcing. *J. Climate*, **34**, 3771–3786, https://doi.org/10.1175/JCLI-D-20-0151.1.

Kajtar, J. B., A. Santoso, M. Collins, A. S. Taschetto, M. H. England, and L. M. Frankcombe, 2021: CMIP5 intermodel relationships in the baseline Southern Ocean climate system and

Brought to you by UNIVERSITY OF CALIFORNIA San Diego - SIO LIBRARY 0219 SERIALS | Unauthenticated | Downloaded 07/02/22 12:17 AM UTC

with future projections. *Earth's Future*, **9**, e2020EF001873, https://doi.org/10.1029/2020EF001873.

Kang, S. M., 2020: Extratropical influence on the tropical rainfall distribution. *Curr. Climate Change Rep.*, **6**, 24–36, https://doi.org/10.1007/s40641-020-00154-y.

——, I. M. Held, D. M. W. Frierson, and M. Zhao, 2008: The response of the ITCZ to extratropical thermal forcing: Idealized slab-ocean experiments with a GCM. *J. Climate*, **21**, 3521–3532, https://doi.org/10.1175/2007JCLI2146.1.

——, Y. Shin, and S.-P. Xie, 2018: Extratropical forcing and tropical rainfall distribution: Energetics framework and ocean Ekman advection. *npj Climate Atmos. Sci.*, **1**, 20172, https://doi.org/10.1038/s41612-017-0004-6.

——, and Coauthors, 2019: Extratropical–Tropical Interaction Model Intercomparison Project (ETIN-MIP): Protocol and initial results. *Bull. Amer. Meteor. Soc.*, **100**, 2589–2606, https://doi.org/10.1175/BAMS-D-18-0301.1.

——, S.-P. Xie, Y. Shin, H. Kim, Y.-T. Hwang, M. F. Stuecker, B. Xiang, and M. Hawcroft, 2020: Walker circulation response to extratropical radiative forcing. *Sci. Adv.*, **6**, eabd3021, https://doi.org/10.1126/sciadv.abd3021.

——, ——, C. Deser, and B. Xiang, 2021: Zonal mean and shift modes of historical climate response to evolving aerosol distribution. *Sci. Bull.*, **66**, 2405–2411, https://doi.org/10.1016/j.scib.2021.07.013.

Kay, J. E., and Coauthors, 2015: The Community Earth System Model (CESM) large ensemble project: A community resource for studying climate change in the presence of internal climate variability. *Bull. Amer. Meteor. Soc.*, **96**, 1333–1349, https://doi.org/10.1175/BAMS-D-13-00255.1.

——, C. Wall, V. Yettella, B. Medeiros, C. Hannay, P. Caldwell, and C. Bitz, 2016: Global climate impacts of fixing the Southern Ocean shortwave radiation bias in the Community Earth System Model (CESM). *J. Climate*, **29**, 4617–4636, https://doi.org/10.1175/JCLI-D-15-0358.1.

Kent, C., R. Chadwick, and D. P. Rowell, 2015: Understanding uncertainties in future projections of seasonal tropical precipitation. *J. Climate*, **28**, 4390–4413, https://doi.org/10.1175/JCLI-D-14-00613.1.

Li, G., and S.-P. Xie, 2014: Tropical biases in CMIP5 multimodel ensemble: The excessive equatorial Pacific cold tongue and double ITCZ problems. *J. Climate*, **27**, 1765–1780, https://doi.org/10.1175/JCLI-D-13-00337.1.

——, ——, and Y. Du, 2016a: A robust but spurious pattern of climate change in model projections over the tropical Indian Ocean. *J. Climate*, **29**, 5589–5608, https://doi.org/10.1175/JCLI-D-15-0565.1.

——, ——, ——, and Y. Luo, 2016b: Effects of excessive equatorial cold tongue bias on the projections of tropical Pacific climate change. Part I: The warming pattern in CMIP5 multimodel ensemble. *Climate Dyn.*, **47**, 3817–3831, https://doi.org/10.1007/s00382-016-3043-5.

Liu, W., A. V. Fedorov, S. P. Xie, and S. Hu, 2020: Climate impacts of a weakened Atlantic meridional overturning circulation in a warming climate. *Sci. Adv.*, **6**, eaaz4876, https://doi.org/10.1126/sciadv.aaz4876.

Long, S.-M., and S.-P. Xie, 2015: Intermodel variations in projected precipitation change over the North Atlantic: Sea surface temperature effect. *Geophys. Res. Lett.*, **42**, 4158–4165, https://doi.org/10.1002/2015GL063852.

——, ——, and W. Liu, 2016: Uncertainty in tropical rainfall projections: Atmospheric circulation effect and the ocean coupling. *J. Climate*, **29**, 2671–2687, https://doi.org/10.1175/JCLI-D-15-0601.1.

Ma, J., and S.-P. Xie, 2013: Regional patterns of sea surface temperature change: A source of uncertainty in future projections of precipitation and atmospheric circulation. *J. Climate*, **26**, 2482–2501, https://doi.org/10.1175/JCLI-D-12-00283.1.

Marshall, J., J. Scott, K. Armour, J. Campin, M. Kelley, and A. Romanou, 2015: The ocean's role in the transient response of climate to abrupt greenhouse gas forcing. *Climate Dyn.*, **44**, 2287–2299, https://doi.org/10.1007/s00382-014-2308-0.

Menary, M. B., L. Hermanson, and N. J. Dunstone, 2016: The impact of Labrador Sea temperature and salinity variability on density and the subpolar AMOC in a decadal prediction system. *Geophys. Res. Lett.*, **43**, 12 217–12 227, https://doi.org/10.1002/2016GL070906.

——, L. C. Jackson, and M. S. Lozier, 2020: Reconciling the relationship between the AMOC and Labrador Sea in OSNAP observations and climate models. *Geophys. Res. Lett.*, **47**, e2020GL089793, https://doi.org/10.1029/2020GL089793.

Schneider, T., 2017: Feedback of atmosphere–ocean coupling on shifts of the intertropical convergence zone. *Geophys. Res. Lett.*, **44**, 11 644–653, https://doi.org/10.1002/2017GL075817.

Seager, R., N. Naik, and G. A. Vecchi, 2010: Thermodynamic and dynamic mechanisms for large-scale changes in the hydrological cycle in response to global warming. *J. Climate*, **23**, 4651–4668, https://doi.org/10.1175/2010JCLI3655.1.

Shi, J.-R., S.-P. Xie, and L. D. Talley, 2018: Evolving relative importance of the Southern Ocean and North Atlantic in anthropogenic ocean heat uptake. *J. Climate*, **31**, 7459–7479, https://doi.org/10.1175/JCLI-D-18-0170.1.

Shiogama, H., S. Emori, N. Hanasaki, M. Abe, Y. Masutomi, K. Takahashi, and T. Nozawa, 2011: Observational constraints indicate risk of drying in the Amazon basin. *Nat. Commun.*, **2**, 253, https://doi.org/10.1038/ncomms1252.

Soden, B. J., and I. M. Held, 2006: An assessment of climate feedbacks in coupled ocean–atmosphere models. *J. Climate*, **19**, 3354–3360, https://doi.org/10.1175/JCLI3799.1.

Song, X., and G. J. Zhang, 2018: The roles of convection parameterization in the formation of double ITCZ syndrome in the NCAR CESM: I. Atmospheric processes. *J. Adv. Model. Earth Syst.*, **10**, 842–866, https://doi.org/10.1002/2017MS001191.

Timmermann, A., and Coauthors, 2007: The influence of a weakening of the Atlantic meridional overturning circulation on ENSO. *J. Climate*, **20**, 4899–4919, https://doi.org/10.1175/JCLI4283.1.

Tomas, R. A., C. Deser, and L. Sun, 2016: The role of ocean heat transport in the global climate response to projected Arctic sea ice loss. *J. Climate*, **29**, 6841–6859, https://doi.org/10.1175/JCLI-D-15-0651.1.

Wang, C., L. Zhang, S. K. Lee, L. Wu, and C. R. Mechoso, 2014: A global perspective on CMIP5 climate model biases. *Nat. Climate Change*, **4**, 201–205, https://doi.org/10.1038/nclimate2118.

Weaver, A. J., and Coauthors, 2012: Stability of the Atlantic meridional overturning circulation: A model intercomparison. *Geophys. Res. Lett.*, **39**, L20709, https://doi.org/10.1029/2012GL053763.

Weijer, W., W. Cheng, O. A.Garuba, A. Hu, and B. T. Nadiga, 2020: CMIP6 models predict significant 21st century decline of the Atlantic meridional overturning circulation. *Geophys. Res. Lett.*, **47**, e2019GL086075, https://doi.org/10.1029/2019GL086075.

Weller, E., C. Jakob, and M. J. Reeder, 2019: Understanding the dynamic contribution to future changes in tropical precipitation

Brought to you by UNIVERSITY OF CALIFORNIA San Diego - SIO LIBRARY 0219 SERIALS | Unauthenticated | Downloaded 07/02/22 12:17 AM UTC

from low-level convergence lines. *Geophys. Res. Lett.*, **46**, 2196–2203, https://doi.org/10.1029/2018GL080813.

Xiang, B., M. Zhao, Y. Ming, W. Yu, and S. Kang, 2018: Contrasting impacts of radiative forcing in the Southern Ocean versus southern tropics on ITCZ position and energy transport in one GFDL climate model. *J. Climate*, **31**, 5609–5628, https://doi.org/10.1175/JCLI-D-17-0566.1.

Xie, S.-P., 2020: Ocean warming pattern effect on global and regional climate change. *AGU Adv.*, **1**, e2019AV000130, https://doi.org/10.1029/2019AV000130.

——, C. Deser, G. A. Vecchi, J. Ma, H. Y. Teng, and A. T. Wittenberg, 2010: Global warming pattern formation: Sea surface temperature and rainfall. *J. Climate*, **23**, 966–986, https://doi.org/10.1175/2009JCLI3329.1.

——, and Coauthors, 2015: Towards predictive understanding of regional climate change. *Nat. Climate Change*, **5**, 921–930, https://doi.org/10.1038/nclimate2689.

Ying, J., P. Huang, T. Lian, and H. Tan, 2019: Understanding the effect of an excessive cold tongue bias on projecting the tropical Pacific SST warming pattern in CMIP5 models. *Climate Dyn.*, **52**, 1805–1818, https://doi.org/10.1007/s00382-018-4219-y.

Zhang, L., T. L. Delworth, W. Cooke, and X. Yang, 2019: Natural variability of Southern Ocean convection as a driver of observed climate trends. *Nat. Climate Change*, **9**, 59–65, https://doi.org/10.1038/s41558-018-0350-3.

Zhang, R., and T. Delworth, 2005: Simulated tropical response to a substantial weakening of the Atlantic thermohaline circulation. *J. Climate*, **18**, 1853–1860, https://doi.org/10.1175/JCLI3460.1.

Zhou, Z.-Q., and S.-P. Xie, 2015: Effects of climatological model biases on the projection of tropical climate change. *J. Climate*, **28**, 9909–9917, https://doi.org/10.1175/JCLI-D-15-0243.1.

Brought to you by UNIVERSITY OF CALIFORNIA San Diego - SIO LIBRARY 0219 SERIALS | Unauthenticated | Downloaded 07/02/22 12:17 AM UTC